Heliyon 10 (2024) e31565

Contents lists available at ScienceDirect

Heliyon

journal homepage: www.cell.com/heliyon

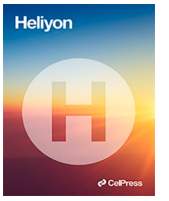

Research article

# Study of graphene incorporation into ZnO-PVA nanocomposites modified electrode for sensitive detection of cadmium

Abrar Ismardi *, Theresia Deviyana Gunawan, Asep Suhendi, Indra Wahyudin Fathona

*Department of Engineering Physics, School of Electrical Engineering, Telkom University, Bandung, Indonesia*

A B S T R A C T

The presence of heavy metals often causes significant health risks, particularly cadmium, which is known for its high toxicity. In this study, a glassy carbon electrode was successfully modified by incorporating ZnO-PVA-Graphene nanocomposite, leveraging the excellent electrical properties and electron mobility of the material. Comprehensive material analysis, including XRD, confirmed that ZnO maintained its hexagonal wurtzite crystal structure despite the addition of graphene. Moreover, FESEM analysis showed that increasing graphene concentration led to a reduction in ZnO particle size by 85, 68, and 52 nm, respectively, accompanied by a decrease in band gap energy, as verified by UV–Vis measurements. Photoluminescence tests were also conducted and the result showed a noticeable blue shift in ZnO-PVA-Graphene nanocomposites compared to ZnO-PVA, specifically in the near band-edge (NBE) UV emission within the 374–379 nm wavelength range. Through I–V characterization, the optimal graphene concentration for cadmium detection was identified as 1.5 wt% in ZnO-PVA-Graphene nanocomposites, showing an approximate ohmic response. Meanwhile, square-wave voltammetry analysis of cadmium concentrations ranging from 0 to 80 ppm produced a coefficient of determination of 0.98926 and a Limit of Detection (LOD) of 9.88 ppm. These results showed the significant potential of ZnO-PVA-Graphene nanocomposites as a promising material for further development as an effective electrode modifier, enhancing the sensitivity of detection systems.

## 1. Introduction

Water is one of the most essential resources for sustaining human life, making the availability of clean water important. With the current rise in industrial activity, there is an accompanying increase in the discharge of industrial effluents containing various unknown inorganic contaminants. Among these contaminants are hazardous heavy metals, including copper (Cu) [1], mercury (Hg) [2], lead (Pb) [3], cadmium (Cd) [4], cobalt (Co) [5], arsenic (As) [6], and iron (Fe) [7]. Even at low concentrations, the heavy metals cause health risks when they accumulate in the human body, leading to issues such as anorexia, hepatitis, nephritis syndrome, kidney damage, insomnia, and cancer [8]. Based on these potential dangers, the United States Environmental Protection Agency (US EPA) established guidelines for maximum industrial effluent discharge standards, including standard concentrations of heavy metals. Cadmium, known for its high toxicity and carcinogenic effects, has a maximum allowable concentration of 0.005 ppm [9]. Despite the widespread applications of cadmium, particularly in battery manufacturing and laboratories, improper disposal and leakage can result in cadmium contaminating the environment [10].

Given the severity of heavy metal contamination, there is a pressing need for highly effective methods to detect even low quantities of the metals. Various methods have been developed for this purpose, including UV–Vis spectrometry, inductively coupled plasma optical emission spectrometry (ICP-OES), electrochemical methods, atomic absorption spectroscopy, and laser-induced breakdown spectroscopy (LIBS) [11]. Among the methods, electrochemical detection was exceptional due to its high sensitivity, accuracy,

* Corresponding author.
*E-mail address:* abrarselah@telkomuniversity.ac.id (A. Ismardi).

https://doi.org/10.1016/j.heliyon.2024.e31565
Received 16 December 2023; Received in revised form 17 May 2024; Accepted 17 May 2024
Available online 18 May 2024
2405-8440/© 2024 The Authors. Published by Elsevier Ltd. This is an open access article under the CC BY-NC license (http://creativecommons.org/licenses/by-nc/4.0/).

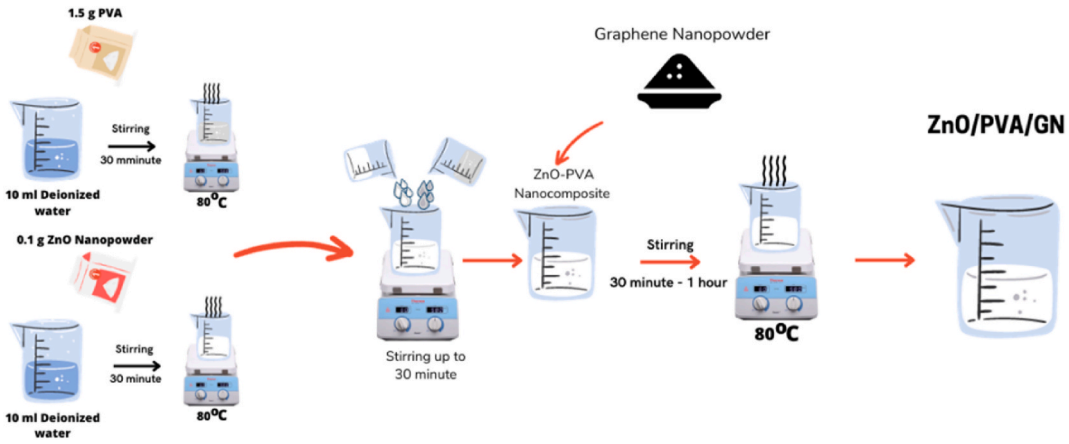


**Fig. 1.** Schematic illustration of the Synthesis process of ZnO-PVA-GN Nanocomposites.

cost-effectiveness, and speed. In electrochemical detection, a supporting electrolyte is used to reduce solution resistance and maintain consistent ionic strength [12]. Several electrolytes such as acetic acid, potassium chloride, sodium chloride, phosphate buffer, and hydrogen chloride are considered the best choices for electrolytes in electrochemical detection [13]. Additionally, the use of a glassy carbon electrode (GCE) is common in heavy metal detection due to its low background current, wide potential range, and ease of use [14]. In this study The utilization of square wave-voltammetry (SWV) was explored to enhance sensitivity and improve data accuracy in heavy metal detection [15].

Metal oxides such as titanium dioxide [16], manganese oxide [17], copper oxide [18], graphene oxide [19], and zinc oxide [20] have been commonly adopted as modifiers in electrochemical detection of heavy metals in water for more than two decades. These oxides possess high selectivity, leading to effectiveness in heavy metal detection [21]. Zinc oxide (ZnO) is particularly interesting for heavy metal detection due to its electrocatalytic capabilities, which are both non-toxic and environmentally friendly. Additionally, the surface of ZnO has numerous hydroxyl groups that enhance contact and sensitivity to cationic analytes bonded by coordination bonds. However, pure ZnO can hinder the electron transfer process, necessitating modification to improve its electrochemical detection abilities [22]. Since ZnO nanoparticles can significantly change polymer characteristics, polymers are incorporated to generate polymer matrix nanocomposites (PMNC) [23].

Polyvinyl alcohol (PVA) is an attractive polymer that needs to be investigated due to its excellent chemical stability, biodegradability, and eco-friendliness. The presence of both an amorphous phase and a crystalline component in PVA creates an interfacial crystal-amorphous effect, improving its physical properties [24]. Combining ZnO-PVA nanocomposite polymers, along with ZnO's role as a filler, changes the optical and electrical properties of PVA as a matrix [25]. Additionally, incorporating ZnO as a filler in a polymer with a large surface area leads to a high aspect ratio. This process improves the characteristics and is accompanied by a quantum confinement effect [8], thereby making nanocomposites with a polymer matrix an interesting subject of study.

Graphene is also selected to create nanocomposites with ZnO in order to improve heavy metal detection abilities. Typically, graphene is a hexagonal lattice-shaped 2D material [26]. that offers unique physical and chemical properties suitable for forming nanocomposites. Additionally, graphene binding to ZnO-PVA nanocomposites increases surface area and forms a material with ultra-high conductivity [22,27]. ZnO-graphene has found utility in various applications, including electrochemical sensors [28].

Previous studies suggest that combining graphene with ZnO in heavy metal detection can increase surface area, while incorporating PVA can improve the material's electrical properties and mechanical strength. However, the application of a ZnO-PVA-Graphene nanocomposite for heavy metal detection has remained unexplored. Therefore, this study proposes a novel method for detecting heavy metals, particularly cadmium, using a ZnO-PVA-Graphene nanocomposite to achieve high sensitivity. In this investigation, ZnO-PVA-Graphene nanocomposites were successfully synthesized and subjected to comprehensive property characterization. I–V characterization showed that nanocomposite with a concentration of 1.5 wt% had a coefficient of determination of 0.989, indicating a close approximation to an ohmic response curve. XRD analysis confirmed that the addition of graphene did not change the crystal structure of ZnO. Moreover, FESEM analysis indicated that increasing graphene concentration resulted in a reduction in the crystal size of ZnO. Optical analysis showed that increasing graphene concentration to 1.5 wt% and 2.5 wt% led to a decrease in band gap energy. Regarding cadmium detection performance, using ZnO-PVA-Nanocomposite with a concentration of 1.5 wt% produced a coefficient of determination value of 0.98926 in the range of 0–80 ppm, with a limit of detection (LOD) of 9.88 ppm.

## 2. Materials and method

### 2.1. Materials

Zinc Oxide nanopowder (<100 nm particle size) was purchased from Sigma Aldrich, Poly-vinyl Alcohol (PVA, 87–90 % hydrolyzed) from Sigma Aldrich, Graphene Nanopowder Multilayer Flakes (C-1) from Graphene Supermarket, and Cadmium Nitrate

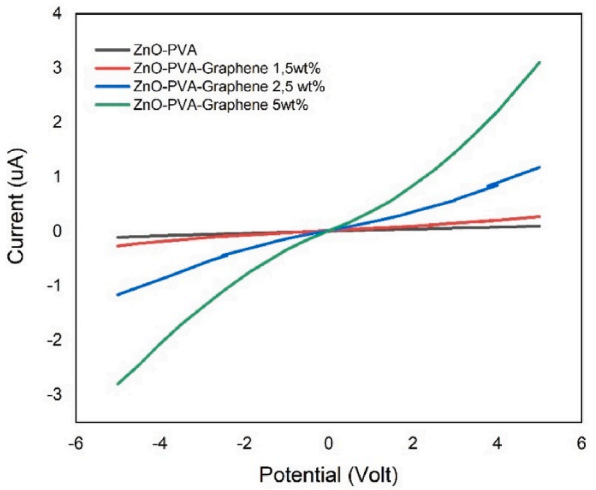


**Fig. 2.** I–V response of ZnO-PVA and ZnO-PVA-Graphene nanocomposites.

Tetrahydrate 99 % from LOBA CHEMIE. Additionally, NaOH was purchased from Sigma Aldrich.

### *2.2. Synthesis of ZnO-PVA-Graphene Nanocomposites*

To synthesize ZnO-PVA nanocomposites, 0.1 g of ZnO were dissolved in 10 ml of distilled water, and 1.5 g of PVA were dissolved in another 10 ml of distilled water. Both mixture were heated on a hotplate and stirred continuously for 30 min at 80 °C to ensure strong bonding between ZnO and PVA. Subsequently, ZnO solution was combined with PVA solution and stirred for an additional 30 min at 80 °C. Graphene nanopowder was then added to ZnO-PVA solution at concentrations of 1.5 wt% and 2.5 wt% and stirred and heated at 80 °C for 30 min. However, for a concentration of 5 wt%, the process was extended to 1 h due to graphene agglomeration. Finally, the ZnO-PVA-Graphene solution was sonicated for 1 h to prevent agglomeration and ensure proper dispersion as shown in Fig. 1.

### *2.3. Characterization*

The electrical properties of ZnO-PVA-Graphene nanocomposite were characterized using Keithley 2400. To determine the crystal structure, X-ray diffractometry was performed using a D8 Advance Eco X-ray diffractometer (Bruker) with Bragg-Bentano Diffraction and a LynxEye XE-T detector, using CuKα radiation (1.54060 Å). Subsequently, field emission scanning electron microscopy (FESEM) was conducted at the Cibinong Science Center, I-Labs Biomaterials, Bogor Indonesia, using a Thermo Scientific Quattro S microscope operating at high vacuum and high voltage (30.0 kV), with magnifications of 50,000×, 80,000×, and 100,000×. Additionally, UV–Vis analysis was carried out at PPBS Padjadjaran University using a Shimadzu UV-1800 UV–Vis Spectrophotometer. Raman spectroscopy, which measures molecular vibrations based on inelastic scattering, was performed at the Serpong Advanced Characterization Laboratory, Banten, Indonesia. Meanwhile, Photoluminescence spectroscopy was conducted at the Integrated Laboratory and Research Center at the University of Indonesia using the Horiba MicOS Photoluminescence instrument, using a 325 nm UV laser light with a wavelength measurement range of 350–1000 nm in steady state.

Regarding electrochemical measurements, a Corrtest CS350 M EIS Potentiostat/Galvanostat was adopted, using Square Wave Voltammetry (SWV). Typically, SWV measurements of $Cd^{2+}$ were carried out with an applied potential ranging from −1.2 V to −0.1 V, a step potential of 10 mV, a frequency of 15 Hz, and an amplitude of 25 mV. All heavy metal solutions were prepared using 0.2 M NaOH as a supporting electrolyte.

### *2.4. Electrode surface modification using ZnO-PVA-Graphene nanocomposites*

Electrode surface modification was prepared using 1 × 1 cm stainless steel, serving as an inert metal for placing ZnO-PVA-Graphene nanocomposites on the working electrode. The ZnO-PVA-Graphene nanocomposite solution went through ultrasonication for 30 min to prevent agglomeration. After ultrasonication, 0.128 g of ZnO-PVA-Graphene nanocomposites were drop-coated onto the stainless steel surface and dried at 45 °C on the hotplate, resulting in a modified electrode with ZnO-PVA-Graphene nanocomposites.

### *2.5. Preparation and testing procedure of cadmium*

The preparation of heavy metal samples comprised 200 ml of distilled water for each cadmium concentration. Subsequently, 0.2 M NaOH was prepared as a supporting electrolyte and stirred until well dispersed at 45 °C for 5 min. Cadmium was then poured into the NaOH electrolyte solution and stirred until well dispersed at 45 °C for 5 min. This process was repeated for each cadmium

**Table 1**
Conductivity and resistance of ZnO-PVA and ZnO-PVA-GN nanocomposites.

| Sample | Conductivity (S) | Resistance (Ohm) |
|---|---|---|
| ZnO-PVA | $1{,}98 \times 10^{-8}$ | $5{,}05 \times 10^{7}$ |
| ZNO-PVA-GN 1.5%wt | $4{,}87 \times 10^{-8}$ | $2{,}05 \times 10^{7}$ |
| ZNO-PVA-GN 2.5%wt | $2{,}08 \times 10^{-7}$ | $4{,}8 \times 10^{6}$ |
| ZNO-PVA-GN 5%wt | $5{,}29 \times 10^{-7}$ | $1{,}89 \times 10^{6}$ |

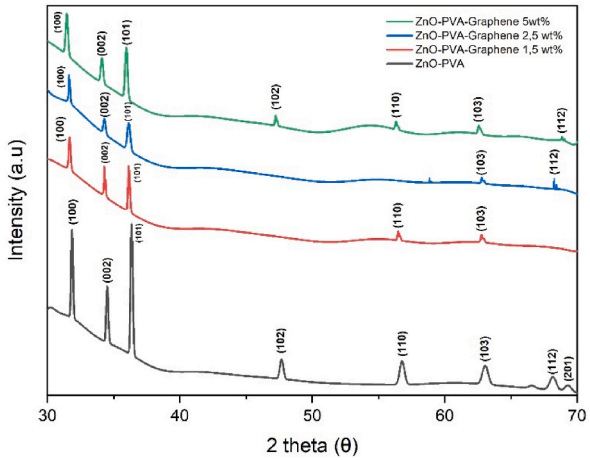


**Fig. 3.** XRD pattern of ZnO-PVA and ZnO-PVA-Graphene nanocomposites [34].

**Table 2**
XRD data of ZnO hkl planes.

| Bragg Angle 2θ (°) | *hkl* | $d_{hkl}$ (Å) |
|---|---|---|
| 31.8 | 100 | 2.80964 |
| 34.5 | 002 | 2.59841 |
| 36.3 | 101 | 2.47155 |
| 47.6 | 102 | 1.90821 |
| 56.6 | 110 | 1.62286 |
| 62.9 | 103 | 1.47517 |
| 68.04 | 112 | 1.37671 |
| 69.1 | 201 | 1.35699 |

concentration.

In this study, cadmium detection was conducted using GCE as electrode and SWV as detection method. Determining the potential range was crucial for studying cadmium detection, with the potential range typically falling within −1.2 V to −0.1 V [29]. Since GCE was used as electrode, attention was paid to the connection from the potentiostat to GCE and the speed of nitrogen purge.

## 3. Results and discussion

### 3.1. I–V characterization of ZnO-PVA-graphene nanocomposites

Fig. 2 showed the I–V curve, indicating the improved electrical conductivity achieved by incorporating graphene into the ZnO-PVA nanocomposite. In the ZnO-PVA-Graphene nanocomposite, semiconductor properties were evident from the graphs, attributed to the semiconductor characteristics of both ZnO and graphene materials. The conductivity values obtained from the I–V curve for each sample of ZnO-PVA nanocomposite and ZnO-PVA-Graphene nanocomposite were shown in Table 1. Additionally, the increased electrical conductivity observed in ZnO-PVA-Graphene nanocomposite samples could be attributed to the increased electron density and mobility of graphene [30]. The formation of a good conductive network by PVA also contributed to increased conductivity, while the uniform dispersion of graphene within the polymer facilitated effective electrical charge storage [31]. The I–V characterization data played a crucial role as a key indicator in advancing electrical devices. The response curve, closely resembling an ohmic curve response, showed efficient charge transfer through the interface of the polymer matrix and electrode [32]. Consequently, the ZnO-PVA-Graphene nanocomposite with a concentration of 1.5 wt%, showing a coefficient of determination of 0.989, was selected for cadmium detection study.

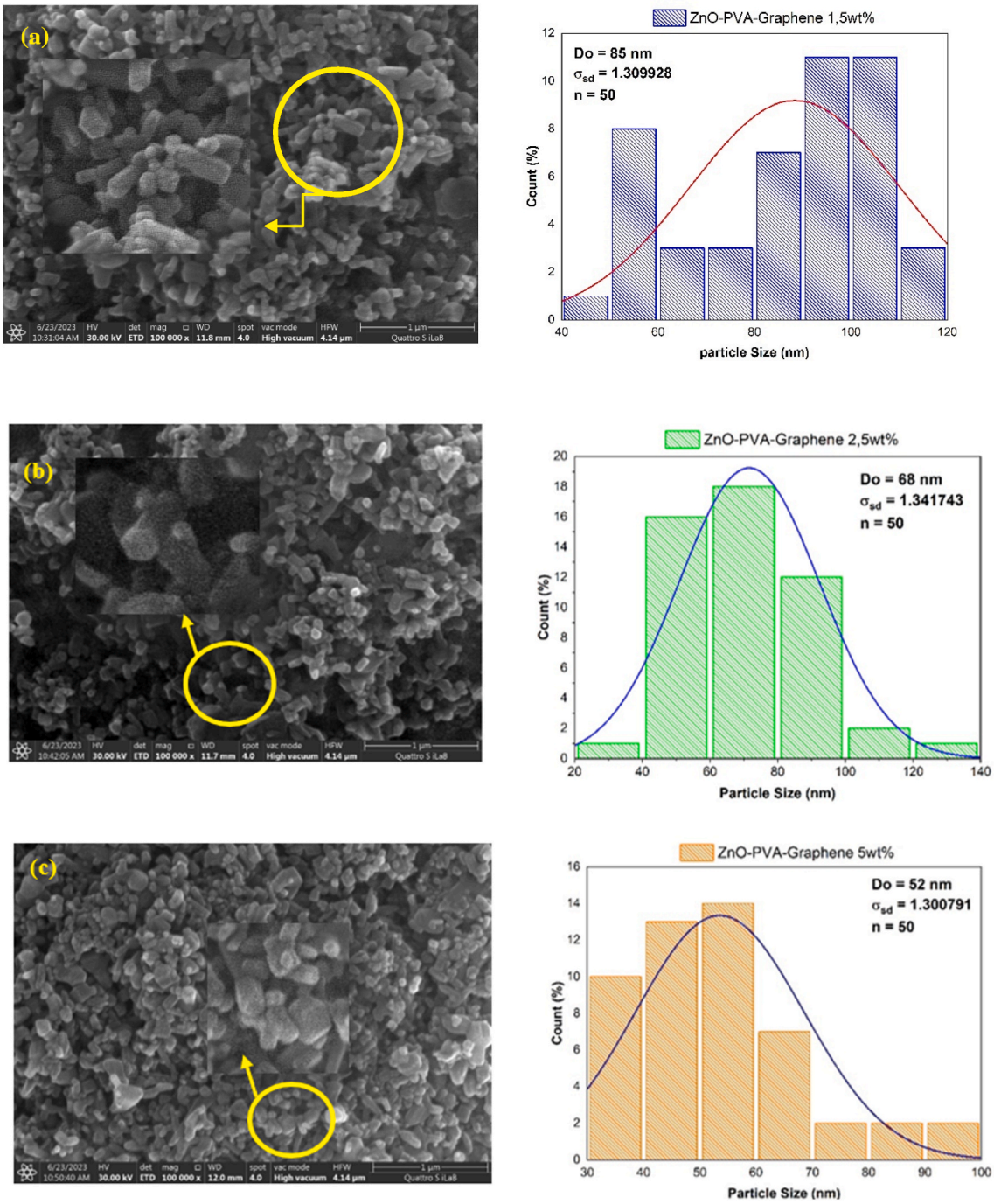


**Fig. 4.** FESEM result of ZnO-PVA-Graphene nanocomposites **(a)** 1,5 wt% **(b)** 2,5 wt% **(c)** 5 wt%.

### *3.2. XRD analysis*

XRD results in Fig. 3 showed that the presence of graphene did not change the crystal structure of ZnO. The distinct peaks of ZnO were observed at 31.8°, 34.5°, 36.3°, 47.6°, 56.6°, 62.8°, 68.1°, and 69.2°, corresponding to the peaks (100), (002), (101), (102), (110), (103), (112), and (201). Sequentially, the XRD peak results showed that ZnO had a hexagonal wurtzite crystal form, consistent with (JCPDS-card No. 36–1451) as shown in Table 2 below [33].

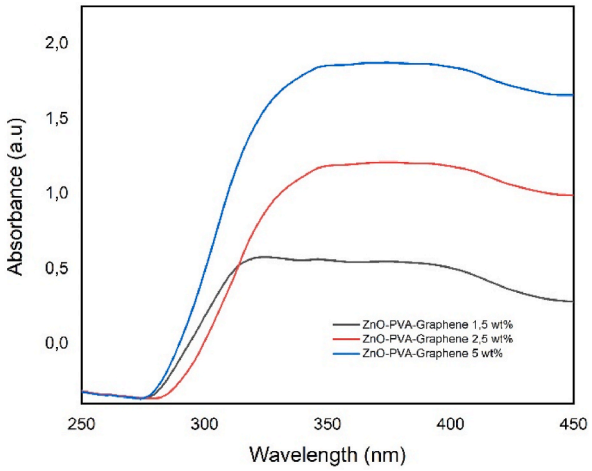


**Fig. 5.** UV–Vis characterization of ZnO-PVA-Graphene nanocomposites.

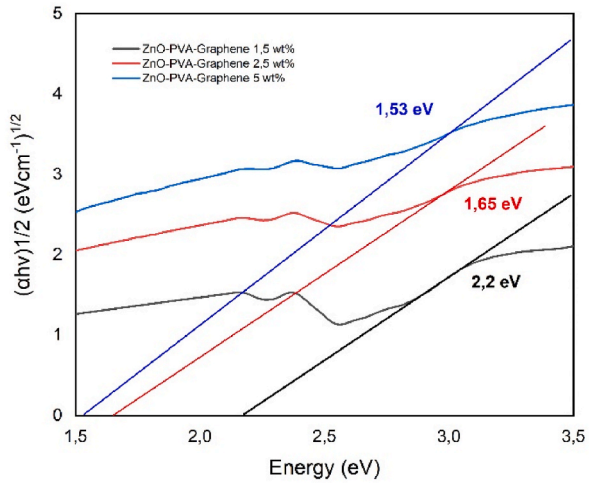


**Fig. 6.** Tauc plots of ZnO-PVA-Graphene nanocomposites.

### *3.3. FESEM analysis*

FESEM results of ZnO-PVA-Graphene nanocomposites, presented in Fig. 4, showed a gradual reduction in the crystal size of ZnO with the addition of graphene. This observation was further confirmed through a histogram plotted using a normal distribution, describing the particle size. The average sizes of ZnO particles were measured at 85 nm, 68 nm, and 52 nm, respectively, as shown in Fig. 4(a–c).

The incorporation of graphene into ZnO-PVA nanocomposites reduced particle size. The synthesis process in ZnO-PVA-Graphene nanocomposites probably had a significant effect on the particle size of ZnO, thereby leading to a decrease in size. This phenomenon could be attributed to the mitigation of dopant-induced grain growth, as supported by prior studies [35–37].

### *3.4. Optical properties investigation*

UV–Vis spectroscopy was conducted on ZnO-PVA-Graphene nanocomposites with three distinct concentrations, as shown in Fig. 5. The characterization results showed the highest absorption peak at a wavelength range of 300–350 nm, attributed to the n-π* transition of the aromatic bond C–C [34]. According to the study report, the visible wavelength for ZnO was 375 nm, which corresponded to a band gap energy of 3.3 eV [38].

The band gap energy of a semiconductor material signifies the energy needed to excite electrons from the valence band to the conduction band. In this instance, the Tauc method was used to precisely ascertain the energy band gap of semiconductor materials. This method assumed that the absorption coefficient depended on the energy α, as expressed in equation (1):

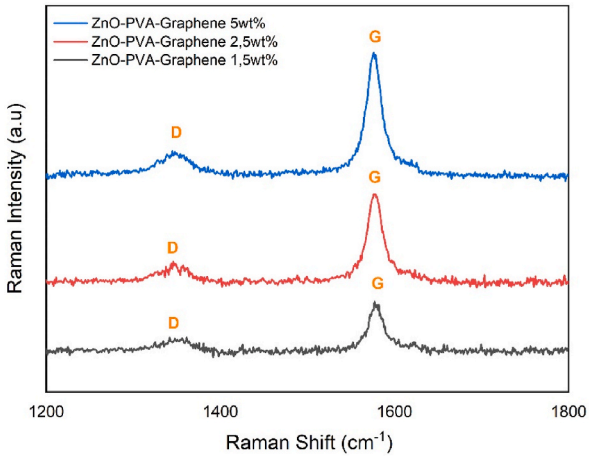


**Fig. 7.** Raman spectroscopy of ZnO-PVA-Graphene nanocomposites.

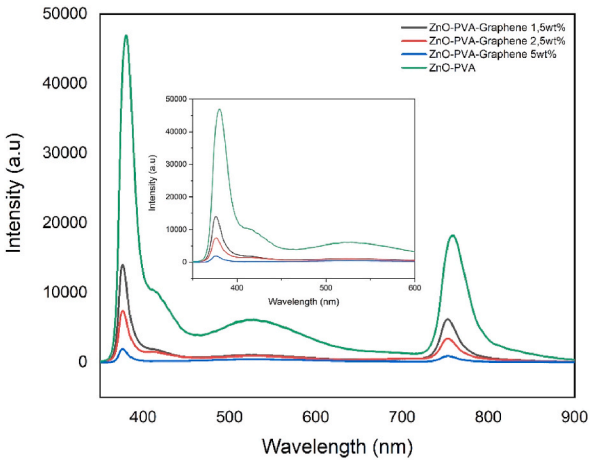


**Fig. 8.** Photoluminescence characterization of ZnO-PVA-graphene nanocomposites.

$$(\alpha.h\nu)^{1/\gamma} = B(h\nu - Eg) \tag{1}$$

where $h$ represented the plank constant, $\nu$ was the photon frequency, $Eg$ denoted the band gap energy, and $B$ signified a constant. Furthermore, the factor $\gamma$ depended on the electron transition, which could be expressed as ½ for direct band gap transitions and 2 for indirect band gap transitions [39]. Fig. 6 showed that the incorporation of graphene into ZnO-PVA nanocomposite could diminish the band gap energy of ZnO compared to pure ZnO with a 3.3 eV direct band gap [34]. The reduction in band-gap energy resulting from the addition of graphene to ZnO-PVA-Graphene suggested that the binding could enhance the absorption and photocatalytic properties of nanocomposite material. Additionally, the decrease in band-gap energy might have arisen from some of the light absorbed by the heterogeneous Zn–*O*–C originating from graphene structure, a type of carbon. This decrease was a consequence of the chemical interaction between ZnO and graphene, leading to a narrowing of the energy band gap [35,40].

To examine the defects in ZnO-PVA-Graphene nanocomposite samples, Raman spectroscopic analysis was conducted, as shown in Fig. 7. The Raman characterization of ZnO-PVA-Graphene nanocomposite showed two prominent peaks at 1344 cm-1 and 1578 cm-1. The peak at 1344 cm-1 was attributed to defects and lattice abnormalities in the D-band orbitals of sp2 C hybridized atoms. Meanwhile, the peak at 1578 cm-1 was attributed to the G-band, resulting from the scattering of E2g phonons and showing a high orientation with the sp2 hexagonal graphite lattice [35,40,41].

Photoluminescence (PL) analysis was carried out to investigate the optical properties of ZnO-PVA and ZnO-PVA-Graphene nanocomposites. In Fig. 8, photoluminescence emission peaks from both ZnO-PVA and ZnO-PVA-Graphene nanocomposites were shown with an excitation wavelength of 325 nm in a steady state. The characterization showed a sharp emission peak in the 374–379 nm range, indicating near band-edge (NBE) UV emission. Additionally, a blue emission at 415 nm was observed, resulting from the transition of electrons from the shallow donor level of the zinc interstitial to the upper part of the valence band. Meanwhile, the green emission at 530 nm was attributed to the transition from oxygen vacancies in ZnO. An increase in concentration led to a decrease in the

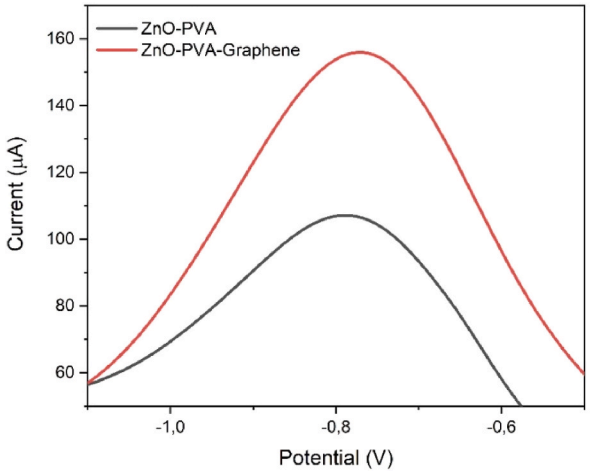


**Fig. 9.** Square-wave voltammogram of ZnO-PVA and ZnO-PVA-Graphene nanocomposites.

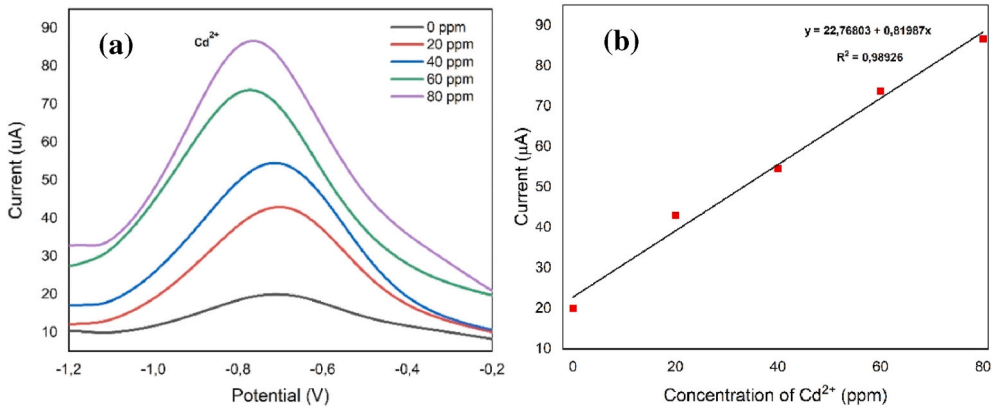


**Fig. 10.** Square-wave voltammetry of ZnO-PVA-Graphene nanocomposites against $Cd^{2+}$ at different concentrations in a range of 0–80 ppm **(a)** Calibration curve of $Cd^{2+}$ between concentrations and current responses **(b)**.

peak intensity of graphene, attributed to charge transfer between graphene and ZnO. Compared to ZnO-PVA nanocomposites, a blue shift occurred, potentially due to the quantum-size effect on the nanometer structure [34,42].

### *3.5. Electrochemical of ZnO-PVA-Graphene Nanocomposites modified electrode*

#### *3.5.1. The analytical sensitivity of electrochemical sensor modified electrode*

The analytical sensitivity of two electrodes, namely ZnO-PVA and ZnO-PVA-Graphene modified electrodes, was investigated for $Cd^{2+}$ detection, as shown in Fig. 9. The square-wave voltammogram for $Cd^{2+}$ detection was recorded on the ZnO-PVA nanocomposite electrode (represented by the black line) and the ZnO-PVA-Graphene nanocomposite electrode (represented by the red line) under alkaline conditions. The potential for $Cd^{2+}$ detection was systematically adjusted within the range of −1.2 V to −0.1 V. Typically, ZnO-PVA-Graphene nanocomposites had a higher response than ZnO-PVA nanocomposites for detection of $Cd^{2+}$. This observation suggested that the integration of graphene with ZnO-PVA nanocomposites successfully enhanced the sensitivity of $Cd^{2+}$ detection under alkaline conditions.

#### *3.5.2. The analytical cadmium detection performance of ZnO-PVA-Graphene nanocomposites*

The performance of detecting cadmium using ZnO-PVA-Graphene nanocomposites was tested in a lab-made solution with NaOH added. Different amounts of $Cd^{2+}$ influenced the changes in SWV peaks, as seen in Fig. 10a. Calibration plots in Fig. 10b showed a straight-line relationship between $Cd^{2+}$ concentration and electrical current responses, indicating accuracy for $Cd^{2+}$ in the range of 0–80 ppm. LOD for $Cd^{2+}$ was calculated using $LOD = 3\,x\left(\frac{SD}{Slope}\right)$ [22], which resulted in 9.88 ppm. While the limited amount of data in this study contributed to a higher LOD for $Cd^{2+}$ compared to previous reports (which reported an LOD of 0.6 ppb), the coefficient of determination showed a strong fit for the model, with a value of 0.98926. This suggested that 98 % of the outcome variation was

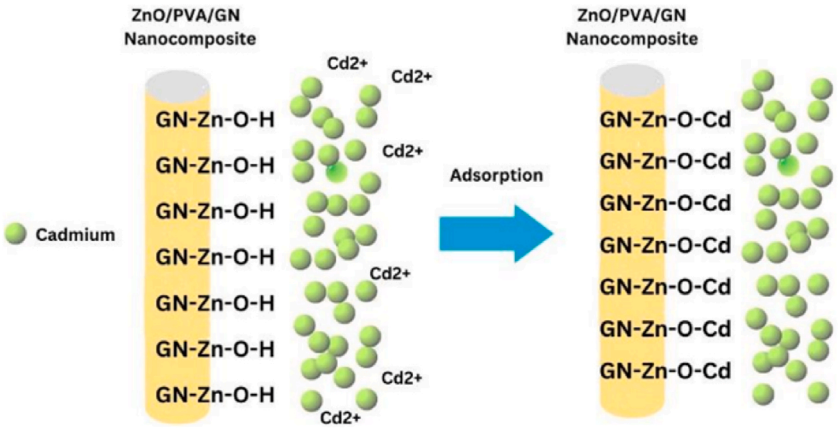


**Fig. 11.** The binding scheme of materials to cadmium.

explained by the model, signifying a robust fit. Consequently, the results of the analytical cadmium detection performance showed that ZnO-PVA-Graphene nanocomposite was beneficial for heavy metal detection.

The process of detecting heavy metals on the surface of ZnO-PVA-Graphene was shown in Fig. 11. This was supported by the bonding formed between the modifier and the target substance. Modifying ZnO increased the negative area, mainly due to the presence of OH- groups [8]. The hydroxyl OH- groups became the primary adsorption sites. The positively charged heavy metal cations in the water solution exhibited a tendency to interact with OH- groups, resulting in the formation of a thin layer on the ZnO particle surface [43].

## 4. Conclusions

In conclusion, ZnO-PVA-Graphene nanocomposites were successfully synthesized and characterized. XRD analysis showed that the addition of graphene did not change the crystal structure of ZnO. Moreover, the incorporation of graphene decreased the particle size of ZnO from 85 nm to 52 nm, as observed using FESEM. Similarly, there was a decrease in the band gap energy to 2.2, 1.65 and 1.53 eV for concentrations of 1.5, 2.5 and 5 wt%, respectively, compared to pure ZnO. Photoluminescence analysis showed a shift towards blue in the ZnO-PVA-Graphene nanocomposite, indicating NBE UV emission between 374 and 379 nm. Regarding detection, ZnO-PVA-Graphene nanocomposite with graphene concentration of 1.5 wt% was selected based on the coefficient of determination obtained from I–V characterization, showing an ohmic curve response conducive to efficient charge transfer. Testing cadmium concentrations ranging from 0 to 80 ppm resulted in a coefficient of determination of 0.98926 and LOD of 9.88 ppm. The results showed the potential of ZnO-PVA-Graphene nanocomposite as a promising material for further development as a modified substrate in heavy metal detection applications. However, using graphene as a doping in ZnO-PVA nanocomposite for cadmium detection application, it should be further researched.

## CRediT authorship contribution statement

**Abrar Ismardi:** Writing – review & editing, Writing – original draft, Validation, Supervision, Resources, Methodology, Funding acquisition, Conceptualization. **Theresia Deviyana Gunawan:** Writing – original draft, Visualization, Project administration, Formal analysis, Data curation. **Asep Suhendi:** Writing – review & editing, Formal analysis, Data curation. **Indra Wahyudin Fathona:** Writing – review & editing, Writing – original draft, Methodology, Formal analysis.

## Declaration of competing interest

The authors declare that they have no known competing financial interests or personal relationships that could have appeared to influence the work reported in this paper.

## Acknowledgements

This study was financially supported by the Kementerian Riset, Teknologi dan Pendidikan Tinggi Indonesia, under grant number 003/SP2H/RTMONO/LL4/2023; 343/PNLT2/PPM/2023.

## References

[1] Z. Shabbir, et al., Copper uptake, essentiality, toxicity, detoxification and risk assessment in soil-plant environment, Chemosphere 259 (2020), https://doi.org/10.1016/j.chemosphere.2020.127436. Elsevier Ltd.

[2] M. Balali-Mood, K. Naseri, Z. Tahergorabi, M.R. Khazdair, M. Sadeghi, Toxic mechanisms of five heavy metals: mercury, lead, Chromium, cadmium, and arsenic, Front. Pharmacol. 12 (Apr. 13, 2021), https://doi.org/10.3389/fphar.2021.643972. Frontiers Media S.A.

[3] F. Cherono, N. Mburu, B. Kakoi, Adsorption of lead, copper and zinc in a multi-metal aqueous solution by waste rubber tires for the design of single batch adsorber, Heliyon 7 (11) (Nov. 2021) e08254, https://doi.org/10.1016/j.heliyon.2021.e08254.

[4] V. Singh, et al., Adsorption studies of Pb(II) and Cd(II) heavy metal ions from aqueous solutions using a magnetic biochar composite material, Separations 10 (7) (Jul. 2023), https://doi.org/10.3390/separations10070389.

[5] R. Wang, L. Deng, X. Fan, K. Li, H. Lu, W. Li, Removal of heavy metal ion cobalt (II) from wastewater via adsorption method using microcrystalline cellulose–magnesium hydroxide, Int. J. Biol. Macromol. 189 (Oct. 2021) 607–617, https://doi.org/10.1016/j.ijbiomac.2021.08.156.

[6] K.M. Nguyen, B.Q. Nguyen, H.T. Nguyen, H.T.H. Nguyen, Adsorption of arsenic and heavy metals from solutions by unmodified iron-ore sludge, Appl. Sci. 9 (4) (Feb. 2019), https://doi.org/10.3390/app9040619.

[7] A. Pinisakul, et al., Arsenic, iron, and manganese adsorption in single and trinary heavy metal solution systems by bamboo-derived biochars, C-Journal of Carbon Research 9 (2) (Jun. 2023), https://doi.org/10.3390/c9020040.

[8] V. Dhiman, N. Kondal, ZnO Nanoadsorbents: a potent material for removal of heavy metal ions from wastewater, Colloids and Interface Science Communications 41 (Mar. 01, 2021), https://doi.org/10.1016/j.colcom.2021.100380. Elsevier B.V.

[9] D.G. Trikkaliotis, et al., Removal of heavy metal ions from wastewaters by using chitosan/poly(vinyl alcohol) adsorbents: a review, Macromol 2 (3) (Aug. 2022) 403–425, https://doi.org/10.3390/macromol2030026.

[10] M. Eftekhari, M. Akrami, M. Gheibi, H. Azizi-Toupkanloo, A.M. Fathollahi-Fard, G. Tian, Cadmium and copper heavy metal treatment from water resources by high-performance folic acid-graphene oxide nanocomposite adsorbent and evaluation of adsorptive mechanism using computational intelligence, isotherm, kinetic, and thermodynamic analyses, Environ. Sci. Pollut. Control Ser. 27 (35) (Dec. 2020) 43999–44021, https://doi.org/10.1007/s11356-020-10175-7.

[11] E.C. Okpara, O.E. Fayemi, O.B. Wojuola, D.C. Onwudiwe, E.E. Ebenso, Electrochemical detection of selected heavy metals in water: a case study of African experiences, RSC Adv. 12 (40) (Sep. 15, 2022) 26319–26361, https://doi.org/10.1039/d2ra02733j. Royal Society of Chemistry.

[12] J. Baranwal, B. Barse, G. Gatto, G. Broncova, A. Kumar, Electrochemical sensors and their applications: a review, Chemosensors 10 (9) (Sep. 01, 2022), https://doi.org/10.3390/chemosensors10090363. MDPI.

[13] E.C. Okpara, S.C. Nde, O.E. Fayemi, E.E. Ebenso, Electrochemical characterization and detection of lead in water using spce modified with bionps/pani, Nanomaterials 11 (5) (May 2021), https://doi.org/10.3390/nano11051294.

[14] E. Sohouli, et al., A glassy carbon electrode modified with carbon nanoonions for electrochemical determination of fentanyl, Mater. Sci. Eng. C 110 (May 2020), https://doi.org/10.1016/j.msec.2020.110684.

[15] V. Mirceski, S. Skrzypek, L. Stojanov, Square-wave voltammetry, ChemTexts 4 (4) (Dec. 2018), https://doi.org/10.1007/s40828-018-0073-0.

[16] T. Ayorinde, C.M. Sayes, An updated review of industrially relevant titanium dioxide and its environmental health effects, Journal of Hazardous Materials Letters 4 (Nov) (2023), https://doi.org/10.1016/j.hazl.2023.100085.

[17] Y. Dessie, S. Tadesse, R. Eswaramoorthy, Review on manganese oxide based biocatalyst in microbial fuel cell: nanocomposite approach, Materials Science for Energy Technologies 3 (Jan. 01, 2020) 136–149, https://doi.org/10.1016/j.mset.2019.11.001. KeAi Communications Co.

[18] A. Waris, et al., A comprehensive review of green synthesis of copper oxide nanoparticles and their diverse biomedical applications, Inorg. Chem. Commun. 123 (Jan. 01, 2021), https://doi.org/10.1016/j.inoche.2020.108369. Elsevier B.V.

[19] H. jiao Qu, et al., A review of graphene-oxide/metal–organic framework composites materials: characteristics, preparation and applications, J. Porous Mater. 28 (6) (Dec. 2021) 1837–1865, https://doi.org/10.1007/s10934-021-01125-w.

[20] I. Constantinoiu, C. Viespe, Zno metal oxide semiconductor in surface acoustic wave sensors: a review, Sensors 20 (18) (Sep. 02, 2020) 1–20, https://doi.org/10.3390/s20185118. MDPI AG.

[21] A.A. Alswata, M. Bin Ahmad, N.M. Al-Hada, H.M. Kamari, M.Z. Bin Hussein, N.A. Ibrahim, Preparation of Zeolite/Zinc Oxide Nanocomposites for toxic metals removal from water, Results Phys. 7 (2017) 723–731, https://doi.org/10.1016/j.rinp.2017.01.036.

[22] J. Yukird, P. Kongsittikul, J. Qin, O. Chailapakul, N. Rodthongkum, ZnO@graphene nanocomposite modified electrode for sensitive and simultaneous detection of Cd (II) and Pb (II), Synth. Met. 245 (Nov. 2018) 251–259, https://doi.org/10.1016/j.synthmet.2018.09.012.

[23] M. Hosseini, H. Rezaei Ashtiani, D. Ghanbari, Production of polymer matrix nanocomposites (PMNC) using various magnetic nanoparticles and investigations of mechanical and physical properties, Trans. Indian Inst. Met. 76 (3) (Mar. 2023) 859–869, https://doi.org/10.1007/s12666-022-02775-3.

[24] S.A. Khan, et al., Performance investigation of ZnO/PVA nanocomposite film for organic solar cell, in: Materials Today: Proceedings, Elsevier Ltd, 2021, pp. 2615–2621, https://doi.org/10.1016/j.matpr.2021.05.197.

[25] T.S. Soliman, A.M. Rashad, I.A. Ali, S.I. Khater, S.I. Elkalashy, Investigation of linear optical parameters and dielectric properties of polyvinyl alcohol/ZnO nanocomposite films, Physica Status Solidi (A) Applications and Materials Science 217 (19) (Oct. 2020), https://doi.org/10.1002/pssa.202000321.

[26] Ababay Ketema Worku, Delele Worku Ayele, Recent advances of graphene-based materials for emerging technologies, Results in Chemistry 5 (Jan. 01, 2023), https://doi.org/10.1016/j.rechem.2023.100971. Elsevier B.V.

[27] A. Machín, et al., Biomimetic catalysts based on Au@ZnO-graphene composites for the generation of hydrogen by water splitting, Biomimetics 5 (3) (Sep. 2020), https://doi.org/10.3390/BIOMIMETICS5030039.

[28] R.R. Sawkar, M.M. Shanbhag, S.M. Tuwar, K. Mondal, N.P. Shetti, Zinc oxide–graphene nanocomposite-based sensor for the electrochemical determination of cetirizine, Catalysts 12 (10) (Oct. 2022), https://doi.org/10.3390/catal12101166.

[29] E.C. Okpara, S.C. Nde, O.E. Fayemi, E.E. Ebenso, Electrochemical characterization and detection of lead in water using spce modified with bionps/pani, Nanomaterials 11 (5) (May 2021), https://doi.org/10.3390/nano11051294.

[30] Ö. Güler, S.H. Güler, O. Başgöz, M.G. Albayrak, I.S. Yahia, Synthesis and characterization of ZnO-reinforced with graphene nanolayer nanocomposites: electrical conductivity and optical band gap analysis, Mater. Res. Express 6 (9) (Jun. 2019), https://doi.org/10.1088/2053-1591/ab2b12.

[31] S. Ningaraju, H.B. Ravikumar, Studies on electrical conductivity of PVA/graphite oxide nanocomposites: a free volume approach, J. Polym. Res. 24 (1) (Dec. 2016), https://doi.org/10.1007/s10965-016-1176-1.

[32] R. Ambrosio, et al., Polymeric nanocomposites membranes with high permittivity based on PVA-ZnO nanoparticles for potential applications in flexible electronics, Polymers 10 (12) (Dec. 2018), https://doi.org/10.3390/polym10121370.

[33] M. Saranya, R. Ramachandran, F. Wang, Graphene-zinc oxide (G-ZnO) nanocomposite for electrochemical supercapacitor applications, J. Sci.: Advanced Materials and Devices 1 (4) (Dec. 2016) 454–460, https://doi.org/10.1016/j.jsamd.2016.10.001.

[34] I. Boukhoubza, et al., Graphene oxide concentration effect on the optoelectronic properties of ZnO/GO nanocomposites, Nanomaterials 10 (8) (Aug. 2020) 1–16, https://doi.org/10.3390/nano10081532.

[35] E. Albiter, A.S. Merlano, E. Rojas, J.M. Barrera-Andrade, Á. Salazar, M.A. Valenzuela, Synthesis, characterization, and photocatalytic performance of zno–graphene nanocomposites: a review, Journal of Composites Science 5 (1) (2021), https://doi.org/10.3390/jcs5010004. MDPI AG.

[36] I. Boukhoubza, M. Khenfouch, M. Achehboune, B.M. Mothudi, I. Zorkani, A. Jorio, Graphene oxide/ZnO nanorods/graphene oxide sandwich structure: the origins and mechanisms of photoluminescence, J. Alloys Compd. 797 (Aug. 2019) 1320–1326, https://doi.org/10.1016/j.jallcom.2019.04.266.

[37] S.L. Dreyer, et al., " the effect of doping process route on LiNiO 2 cathode material properties ,", J. Electrochem. Soc. 170 (6) (Jun. 2023) 060530 https://doi.org/10.1149/1945-7111/acdd21.

[38] K. Davis, R. Yarbrough, M. Froeschle, J. White, H. Rathnayake, Band gap engineered zinc oxide nanostructures: via a sol-gel synthesis of solvent driven shape-controlled crystal growth, RSC Adv. 9 (26) (2019) 14638–14648, https://doi.org/10.1039/c9ra02091h.

[39] P. Makuła, M. Pacia, W. Macyk, How to correctly determine the band gap energy of modified semiconductor photocatalysts based on UV-vis spectra, J. Phys. Chem. Lett. 9 (23) (Dec. 06, 2018) 6814–6817, https://doi.org/10.1021/acs.jpclett.8b02892. American Chemical Society.

[40] S. Alamdari, et al., Preparation and characterization of GO-ZnO nanocomposite for UV detection application, Opt. Mater. 92 (Jun. 2019) 243–250, https://doi.org/10.1016/j.optmat.2019.04.041.

[41] A.N. Fouda, A.B. El Basaty, E.A. Eid, Photo-response of functionalized self-assembled graphene oxide on zinc oxide heterostructure to uv illumination, Nanoscale Res. Lett. 11 (1) (2016), https://doi.org/10.1186/s11671-015-1221-8. Springer New York LLC.
[42] P. Kumar, S. Som, M.K. Pandey, S. Das, A. Chanda, J. Singh, Investigations on optical properties of ZnO decorated graphene oxide (ZnO@GO) and reduced graphene oxide (ZnO@r-GO), J. Alloys Compd. 744 (May 2018) 64–74, https://doi.org/10.1016/j.jallcom.2018.02.057.
[43] A. Thi Le, S.-Y. Pung, S. Sreekantan, A. Matsuda, D. Phu Huynh, D. Phu Huynh Mechanisms, Mechanisms of removal of heavy metal ions by ZnO particles, Heliyon 5 (2019) e01440, https://doi.org/10.1016/j.heliyon.2019.